Environmental Science and Pollution Research (2019) 26:3455–3464
https://doi.org/10.1007/s11356-018-3821-1

RESEARCH ARTICLE

Amalgamation of N-graphene quantum dots with nanocubic like TiO_2: an insight study of sunlight sensitive photocatalysis

Ping Feng Lim[1] · Kah Hon Leong[1] · Lan Ching Sim[2] · Azrina Abd Aziz[3] · Pichiah Saravanan[4]

Received: 20 August 2018 / Accepted: 21 November 2018 / Published online: 4 December 2018

Abstract

In this work, a sunlight-sensitive photocatalyst of nanocubic-like titanium dioxide (TiO_2) and N-doped graphene quantum dots (N-GQDs) is developed through a simple hydrothermal and physical mixing method. The successful amalgamation composite photocatalyst characteristics were comprehensively scrutinized through various physical and chemical analyses. A complete removal of bisphenol A (BPA) is attained by a synthesized composite after 30 min of sunlight irradiation as compared to pure TiO_2. This clearly proved the unique contribution of N-GQDs that enhanced the ability of light harvesting especially under visible light and near-infrared region. This superior characteristic enables it to maximize the absorbance in the entire solar spectrum. However, the increase of N-GQDs weight percentage has created massive oxygen vacancies that suppress the generation of active radicals. This resulted in a longer duration for a complete removal of BPA as compared to lower weight percentage of N-GQDs. Hence, this finding can offer a new insight in developing effective sunlight-sensitive photocatalysts for various complex organic pollutants degradation.

Keywords N-Graphene quantum dots · Nanocubic-like TiO_2 · Bisphenol A · Sunlight · Visible light · Near Infrared

Introduction

Bisphenol A (BPA) is a man-made endocrine chemical compound which is extensively used as raw material in polycarbonate plastics and epoxy resins production (Zhao et al. 2014; Bechambi et al. 2016; Dominguez et al. 2017). These compounds are widely used in various industries especially electrical and electronic appliances, protective coating, and plastic-related industries (Guerra et al. 2015). According to Vandenberg et al., approximately 8 billion pounds of BPA is being produced every year. The rapid growth of these industrial applications has increased the amount of BPA released into the environment, resulting in ubiquitous distribution in the natural water (Wu et al. 2016). Currently, existing conventional treatment methods of BPA that are being applied in the industries (as shown in Table S1) such as biological treatment and adsorption have shown good efficiencies, yet they are not able to achieve complete removal of the pollutant (Yamanaka et al. 2008; Liu et al. 2009; Chai et al. 2012; Taheri et al. 2017). Hence, research and development are continuously carried out to find a better and reliable treatment method.

Heterogeneous photocatalytic oxidation is a promising green technology for water and wastewater treatment, particularly in the application of nano-photocatalyst (Rajabi and Farsi 2015). Among the various photocatalysts, nanosized titanium dioxide is the most commonly used in this field due to its high photosensitivity under UV light, low cost, nontoxic, chemically inert, thermal stability, and readily available (Hund-Rinke and Simon 2006; Henderson 2011; Pelaez

Responsible editor: Suresh Pillai

Electronic supplementary material The online version of this article (https://doi.org/10.1007/s11356-018-3821-1) contains supplementary material, which is available to authorized users.

✉ Kah Hon Leong
khleong@utar.edu.my

[1] Department of Environmental Engineering, Faculty of Engineering and Green Technology, Universiti Tunku Abdul Rahman, 31900 Kampar, Perak, Malaysia

[2] Department of Chemical Engineering, Lee Kong Chian Faculty of Engineering and Science, Universiti Tunku Abdul Rahman, Jalan Sungai Long 9, Bandar Sungai Long, 43000 Kajang, Selangor, Malaysia

[3] Department of Energy and Environment, Faculty of Engineering Technology, Universiti Malaysia Pahang, Lebuhraya Tun Razak, 26300 Gambang, Kuantan, Pahang, Malaysia

[4] Environmental Nanotechnology Laboratory, Department of Environmental Science and Engineering, Indian Institute of Technology (ISM), Dhanbad, Jharkhand 826004, India

et al. 2012; Park et al. 2013; Grabowska et al. 2017). TiO_2 exhibits several polymorphs and sizes. Owing to its unique structures, a theory claimed by Mahmood et al. 2013 stated that the cubic-phase TiO_2 can exhibit better light absorption in the visible range (Miloua et al. 2011; Mahmood et al. 2013). Furthermore, Xu et al. proved that cubic TiO_2 can display high photocatalytic efficiency due to its synergetic effects of improving crystallization and a greater amount of co-exposed facets. The exposed facets of cubic TiO_2 are believed to offer more active sites for pollutant adsorption and allow more reductive electrons and oxidative holes for photocatalysis (Roy et al. 2013; Xu et al. 2015). The application of TiO_2 shows good photocatalytic activity and high degradation rate in low levels of contaminants (Chong et al. 2015). However, the extensive use of TiO_2 photocatalysts in large-scale water treatment possesses has a few drawbacks. The efficiency is often low due to its undesirable high recombination rate of photogenerated electron-hole pairs (h^+/e^-). In addition, TiO has poor photon absorption ability in the visible light region due to its wide band gap energy (3.2 eV). Therefore, it is merely active in the ultraviolet (UV) region and only accountable for approximately 4% of sunlight. This resulted in low quantum efficiency (Amorós-Pérez et al. 2017; Chen et al. 2017).

Many efforts and researches are performed to overcome all these drawbacks. Common approaches such as doping with metal or non-metal elements, interstitial atoms like nitrogen (N) or sulfur (S), hydrogen annealing, and chalcogenide materials (CdS, CdSe, PbS, etc.) with the aim to narrow down the band gap energy and expand to higher light utilization (Wang et al. 2011; Rodenas et al. 2013; González-Pedro et al. 2014; Ribao et al. 2017) are performed. However, some of these materials used may cause a severe threat to the environment. Thus, it is important to look into a substituent material which is environmentally friendly and able to address all these drawbacks. Recently, the application of heterogeneous quantum dots such as ZnS as well as graphene quantum dots (GQDs) for catalytic degradation of organic pollutants is widely studied (Rajabi et al. 2013; Roushani et al. 2015; Rajabi and Farsi 2016). GQDs are a newly emerging candidate which received significant attention in photocatalysis and photoelectrochemical conversion (Chimmikuttanda et al. 2017; Safardoust-Hojaghan and Salavati-Niasari 2017). GQDs are a small disk of graphene sheets with size less than 20 nm and this fluorescent carbon nanomaterial is mainly composed of sp^2 hybridized carbon (Dong et al. 2014). GQDs are renowned for its ultraviolet and blue to green luminescence, excellent photostability, high electron reservation capability, biocompatibility, tunable optical and electronic properties, plentiful edge defects, chemical inertness, and environmentally benign and cost-effective preparation (Chan et al. 2014; Pan et al. 2015; Min et al. 2017). Besides that, GQDs can be used directly as a metal-free photocatalyst to modify nanoparticle semiconductors with an enhanced photocatalytic performance by reducing photoelectron loss (Das et al. 2016).

Inspired by these considerations, the principle aim of this research is to focus on modification of nanocubic-like TiO_2 incorporated with N-GQDs to synergize visible and NIR light utilization for enhanced sunlight photocatalysis and prolong the lifetime of the charge carriers. Hence, the present work demonstrates the synthesis of TiO_2 and N-GQDs through the hydrothermal and physical mixing process. This sunlight-sensitive photocatalyst can provide a new insight into the degradation of BPA under sunlight irradiation.

Experimental

Materials

Titanium (IV) butoxide (TBT) (97%, Sigma Aldrich, USA), citric acid ($C_6H_8O_7$) anhydrous (chemically pure, R & M Chemicals, UK), urea (NH_2CONH_2) (R & M Chemicals, UK), absolute ethanol (C_2H_5OH, 95%,), isopropyl alcohol (99%) (Hmbg Chemicals, Germany), dimethyl sulphoxide (99%, UNIVAR, Australia), p-benzoquinone (98%, Sigma Aldrich, USA), ethylenediaminetetraacetic acid disodium (99%, ChemSoln, Malaysia), and deionized water. All chemicals used in this experiment were of analytic purity and were used without further purification.

Preparation of nanocubic-like TiO_2, N-GQDs, and modified N-GQDs/TiO_2 nanocube

Nanocubic-like TiO_2 was synthesized by the simple hydrothermal method. Specifically, 1 mmol of titanium (IV) butoxide was mixed in 5 ml of ethanol with 2 h continuous stirring until an immediate white precipitate was formed. The as-prepared solution was aged at room temperature for 48 h. The aged solution was further heated at 100 °C for 48 h in a Teflon-lined stainless-steel autoclave. The resulting products were centrifuged and washed with deionized water and ethanol. Then, the photocatalysts were dried in an oven at 70 °C overnight.

The N-GQDs solution was obtained by a single-step hydrothermal method. One millimole of citric acid and 3 mmol of urea were dissolved in 5 ml deionized water. The mixture was stirred to form a clear solution. The mixture was then transferred into a Teflon-lined stainless-steel autoclave and heated at 160 °C for 8 h. The final product was kept in liquid form as N-GQDs is easily dispersed in water.

The deposition of N-GQDs on the surface of nanocubic-like TiO_2 was performed through a simple physical mixing route. The deposition was achieved by varying the weight percentage ratio of N-GQDs (0.5%, 1.5%, and 2.5%) onto TiO_2. 0.5 g of nanocubic-like TiO_2 was dispersed into 7 ml,

20 ml, and 35 ml of N-GQDs aqueous solution respectively and stirred for 24 h at ambient temperature. The resulting products were collected by centrifugation at 5000 rpm for 30 min and dried at 70 °C.

Characterization of N-GQDs/TiO_2 nanocube

The morphology of the composite was investigated by a field emission scanning electron microscope (FESEM, Hitachi SU-8000) equipped with an energy dispersive X-ray spectroscopy (EDS, Zeiss Auriga). The images were recorded at an accelerating voltage of 20 kV. High-resolution transmission electron microscope (HRTEM, JEM-2100F, Jeol) images were obtained at 200 kV. The crystalline and phase compositions were analyzed by X-ray diffraction (XRD, Bruker D8 advance X-ray powder diffractometer with Cu Kα radiation $\lambda =$ 0.154 nm). A micro-PL/Raman spectroscope with the excitation wavelength at 514 nm and 325 nm (Renishaw, inVia Raman Microscope) was used to acquire photoluminescence (PL) and Raman spectra. Fourier transform infrared (FTIR) spectrums were obtained by Perkin Elmer Spectrum 400 spectrophotometer with a scan range of 4000–450 cm^{-1}. X-ray photoelectron spectra (XPS) was obtained with Axis Ultra DLD instrument of Kratos using monochromatic AlKα radiation (225 W, 15 mA, 15 kV). The C1s binding energy of adventitious carbon (284.9 eV) was used as a reference. UV-Vis diffuse reflectance spectra (UV-DRS) were performed through Shimadzu UV-2600 spectrophotometer equipped with an integrating sphere attachment to characterize the optical properties. The absorption spectra were obtained with $BaSO_4$ as a reference.

Photocatalytic activities

The prepared photocatalysts were evaluated through photocatalysis by utilizing sunlight as a source of irradiation. A poor photosensitizing pollutant, BPA was prepared in a 500-mL borosilicate beaker filled with 250 mL of working volume with 20 ppm as initial concentration. Photocatalysis was performed with 1 g of photocatalyst dispersed in the BPA solution. Prior to the reaction, the mixture was carried out in a dark condition for 24 h to achieve adsorption and desorption equilibrium before treatment under sunlight with intensities between 40,000 and 100,000 Lux (approximately 60–150 Wm^{-2}) for a duration of 60 min. A control experiment was carried out without the presence of a photocatalyst to ensure the photodegradation is contributed by the presence of photocatalysts. The residual concentration of BPA solution samples was analyzed by Perkin Elmer high-performance liquid chromatography (HPLC). The active radical species were obtained through scavenger test. Isopropanol (IPA), ethylenediaminetetraacetic acid disodium salt (EDTA-2Na), and benzoquinone (BQ) were added into the BPA solution containing a photocatalyst to inhibit hydroxyl radical (·OH), holes (h^+), and superoxide anion radical ($\cdot O_2^-$), respectively.

Results and discussion

Characterization of N-GQDs/TiO_2 nanocubic composites

The crystal structure of N-GQDs/TiO_2 was studied by XRD analysis and the results are shown in Fig. 1. The XRD patterns of nanocubic-like TiO_2 and N-GQDs/TiO_2 are detected at diffraction peaks 2θ appearing at 25.4°, 38.36°, 48.12°, 55.18°, and 62.9°. These peaks are attributed to (101), (004), (200), (105), and (204), respectively, in which all these peaks are well matched with the JCPDS Card No. 21-1272. It also corresponded to the lattice plane of the anatase phase of TiO_2 (Leong et al. 2014; Tian et al. 2017; Huy et al. 2017; Li et al. 2018). It is noteworthy that N-GQDs/TiO_2 composites exhibit a similar pattern to the pristine TiO_2 and this proves the deposition of N-GQDs onto TiO_2 does not affect its crystal structure (Yu et al. 2016; Xie et al. 2017). The absence of any additional diffraction peaks further indicates the high purity of the composite. The diffraction peak of graphene (002) at 26.6° is shielded by the anatase TiO_2 peak (101) with similar findings also reported by other researchers (Martins et al. 2016; Shen et al. 2017; Tian et al. 2017).

Figure 2 illustrates the morphology of 0.5 N-GQDs/TiO_2 composite through FESEM imaging. It is clearly shown that TiO_2 prepared through the hydrothermal method is well composed of cubic shape and regular outline. The as-prepared nanocomposites show a porous cubic like morphology is

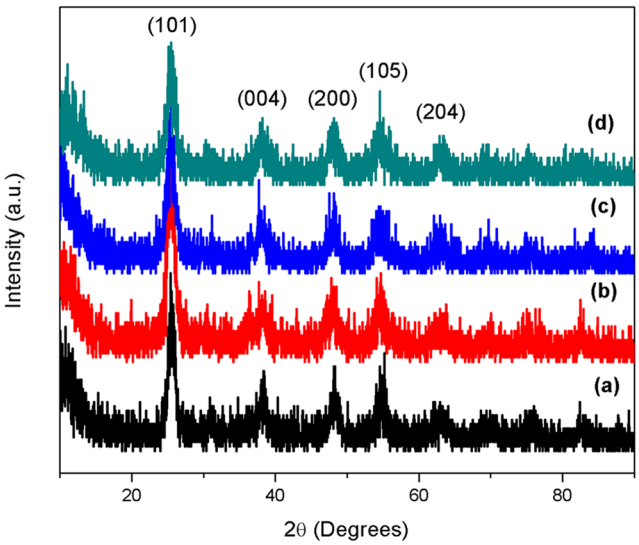

Fig. 1 XRD diffraction pattern of **a** TiO_2, **b** 0.5 N-GQDs/TiO_2, **c** 1.5 N-GQDs/TiO_2, and **d** 2.5 N-GQDs/TiO_2

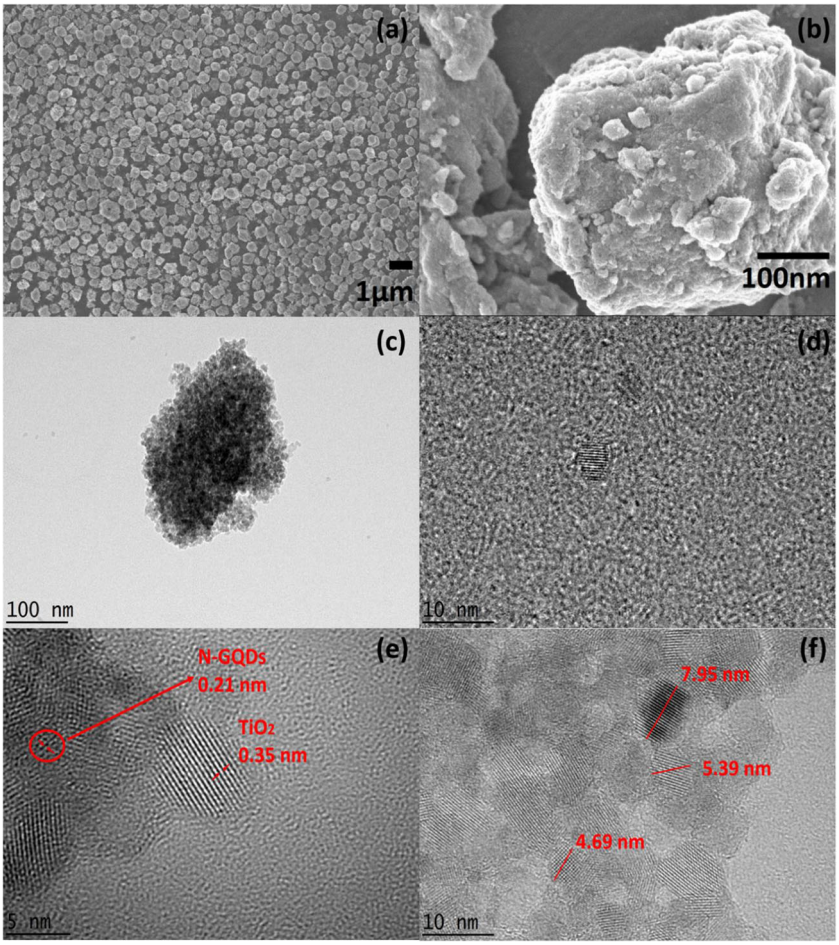

Fig. 2 **a**, **b** FESEM images; **c**, **d** HRTEM images; and **e**, **f** lattice fringes of 0.5 N-GQDs/TiO_2

mainly due to the formation of TiO_2 cluster (Shen et al. 2017). The chemical elements of the composites are shown in Fig. S1 through the EDX analysis. It visibly shows strong signals from titanium and oxygen atoms, whereas the low intensity of carbon atom attributed to N-GQDs. Meanwhile, Fig. 2 c–f shows HRTEM images of N-GQDs deposited onto TiO_2. It is evident that deposition is well dispersed in narrow size distribution without any apparent aggregation. Furthermore, Fig. 2 e, f indicates high crystallinity of N-GQDs with discernible lattice fringes with a spacing of 0.21 nm proving the presence of graphite and are consistent with the (1 0 2) diffraction planes of sp^2 graphitic carbon (Zhu et al. 2015). Moreover, the lattice fringes of 0.35 nm attributed to the presence of nanocubic-like TiO_2 which corresponds to (1 0 1) plane of TiO_2 (Xu et al. 2015). Therefore, the deposition of N-GQDs with TiO_2 does not change the morphology of TiO_2 which also match well with the XRD results (Xie et al. 2017).

Figure 3 shows FTIR spectra of the prepared composites with broad absorption bands at 3000–3500 cm^{-1} that is attributed to the O–H stretching vibrational absorptions and N–H bonds. This suggests that there are numerous hydroxyl and amino groups present on the surface of the N-GQDs/TiO_2. The strong intensity peak at 1671 cm^{-1} is associated with the C=O stretching vibration in COOH and the weak band at 1400 cm^{-1} corresponded to the stretching vibration of C–N where both of these peaks are mainly due to the presence of N-

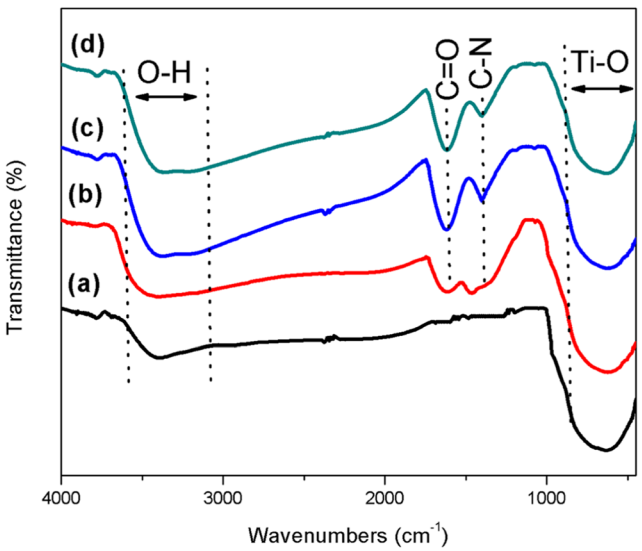

Fig. 3 FTIR spectra of **a** TiO_2, **b** 0.5 N-GQDs/TiO_2, **c** 1.5 N-GQDs/TiO_2, and **d** 2.5 N-GQDs/TiO_2 composite

GQDs. The existence of metal oxide bands Ti–O and Ti–O–Ti stretching vibrations are observed in the range of 500–700 cm^{-1}. These spectrums prove the as-prepared N-GQDs/TiO_2 contains COOH and N-containing functional groups that will result to a good hydrophilic property and leads to an enhanced photocatalysis (Pan et al. 2010; Kaur and Verma 2014).

XPS analysis was performed to identify the chemical compositions and surface properties of N-GQDs/TiO_2 and is shown in Fig. 4. It clearly shows four distinct peaks that correspond to O 1s, N 1s, C 1s, and Ti 2p. The peak Ti 2p shows two prominent peaks at 458.3 eV and 464.0 eV, which corresponded to the binding energies of Ti $2p_{3/2}$ and Ti $2p_{1/2}$ electrons respectively. The high-resolution scan of the C 1s region shows four carbon peaks present at different chemical environments which are 284.2, 285.3, 286.0, and 288.2 eV, attributed to C–C, C–O, C=O, and COOH groups, respectively, were mainly contributed by N-GQDs. Meanwhile, the O 1s core-level spectrum shows the presence of Ti–O peak at 529.5 eV, C–O signal at 530.5 eV, and COOH at 531.3 eV. The binding energy peak position supported the Ti 2p and C 1s core-level fitting results as most of the oxygen is bonded through Ti–O and C–O of N-GQDs/TiO_2, through the conjunction of Ti–O–C bond (Chua et al. 2015; Pan et al. 2015). The presence of oxygen-containing groups caused the obtained N-GQDs easily disperse in water favorable for the uniform deposition of N-GQDs onto nanocubic-like TiO_2. As seen from the N 1s spectra, three peaks are obtained at 399.7, 400.4, and 401.2 eV. The main peak at 399.7 eV is attributed to the pyrrolic N, a substitution of nitrogen with some lattice oxygen. Meanwhile, the peaks at 400.4 and 401.2 eV are attributed to N–H bands. The N peak indicates that GQDs are doped with N which was obtained from urea during synthesis (Qu et al. 2013). These XPS results are relatively consistent with the FTIR results and it can prove the existence of N-GQDs in the composites without any impurities.

The UV-Vis absorption spectra of the N-GQDs/TiO_2 nanocubic composites with different weight percentage are shown in Fig. 5. The spectrum of TiO_2 shows strong enhancement of absorption that appears at 420 nm which is mainly

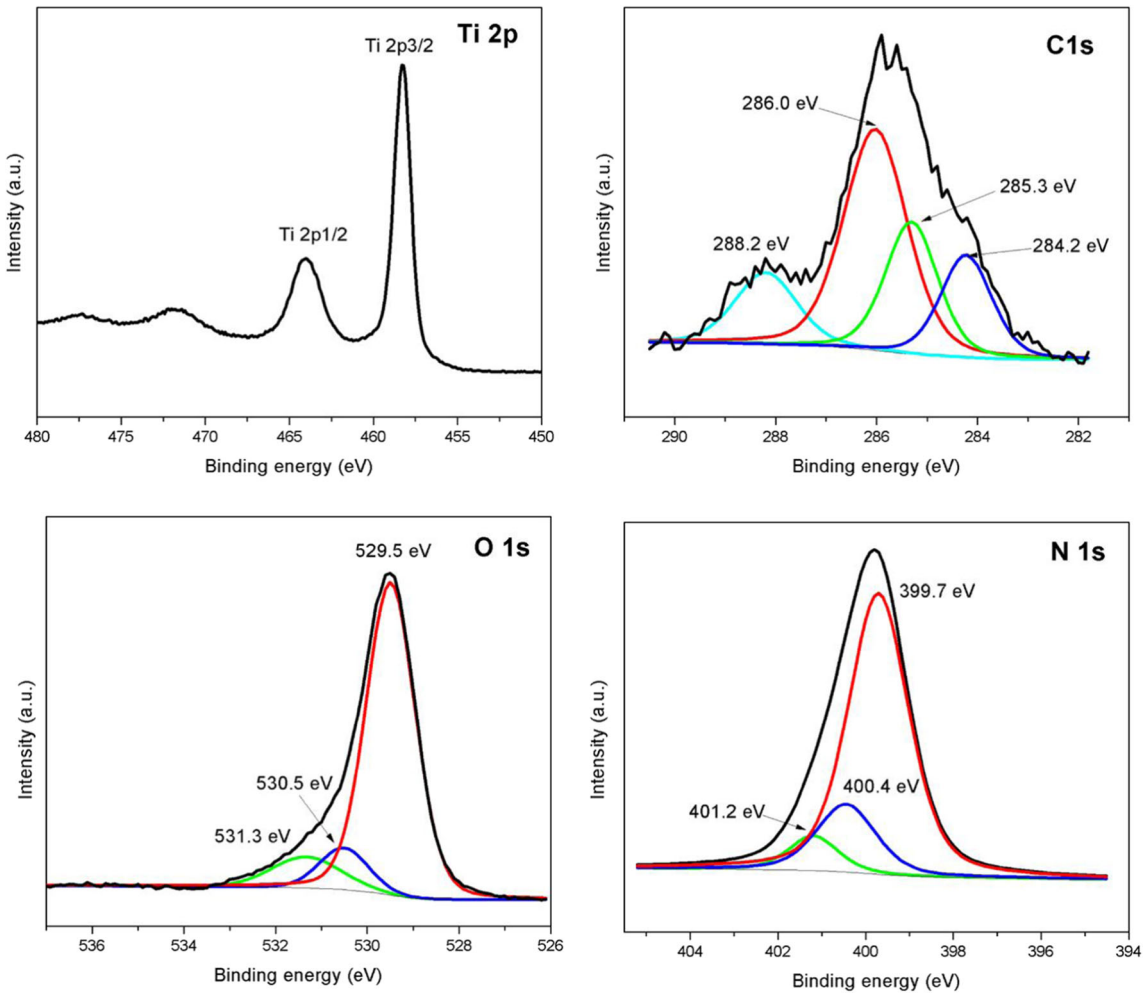

Fig. 4 XPS analysis of N-GQDs/TiO_2 spectra of Ti 2p, C1s, O1s, and N1s

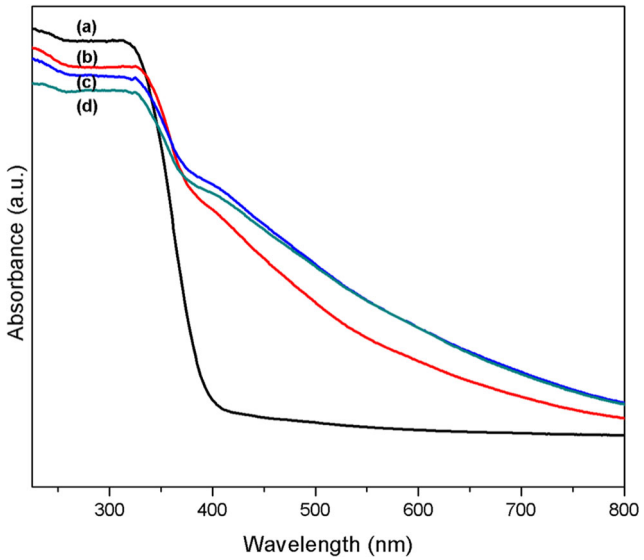

Fig. 5 UV-Vis absorption spectra of **a** TiO_2 and different weight percentage **b** 0.5, **c** 1.5, and **d** 2.5 N-GQDs/TiO_2 samples

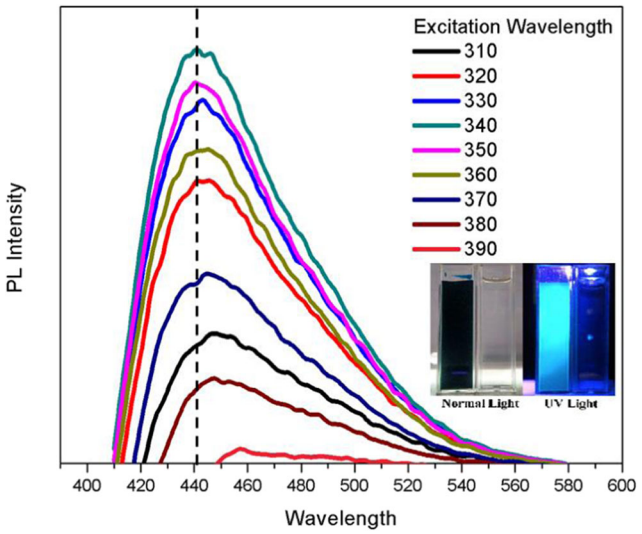

Fig. 6 Photoluminescence (PL) spectra of N-GQDs under different excitations of 310–390 nm. The insert is the optical images of concentrated N-GQDs aqueous solution

caused by excitations of electrons from the valence band to the conduction band of titania (Leong et al. 2014). The obtained spectrum also indicates an obvious red shift in the absorption edge after the deposition of N-GQDs onto TiO_2. This further extended the photoresponse to visible light and near-infrared (NIR) range which is primarily due to the broad absorption ability of N-GQDs that extends to 700 nm (Yu et al. 2016). It is evident that the existence of N-GQDs in the composite contributed to the narrowing of the band gap energy. The optical direct band gap energy of N-GQDs/TiO_2 is calculated using the Kubelka-Munk equation as shown in Fig. S2. The band gap energy of TiO_2, 0.5 N-GQDs/TiO_2, 1.5 N-GQDs/TiO_2, and 2.5 N-GQDs/TiO_2 are estimated to be about 3.4, 3.1, 2.9, and 2.75 respectively. Thus, the narrowing of the TiO_2 band gap energy can be attributed to the synergetic absorption effect of depositing with N-GQDs, which has a chemical bonding through co-doping with N. In brief, a more efficient utilization of the solar spectrum can be achieved with the incorporation of N-GQDs (Shen et al. 2017; Xie et al. 2017).

Figure 6 shows photoluminescence (PL) of N-GQDs under different excitations from 310 to 390 nm. The corresponding PL spectra show maximum emission peak was achieved with an excitation wavelength of 340 nm. PL peak intensity increases with excited wavelength from 310 to 340 nm and then decreases when excited the wavelength rises. No evident shift is observed under the excitation wavelength from 310 to 360 nm. However, when the excitation wavelength changes from 360 to 390 nm, PL peaks red-shifted to a longer wavelength with wider bands and rapid decrement of intensity. The photoluminescence red shift of N-GQDs with a reduction in PL intensity elucidates the excitation-dependent PL behavior of N-GQDs, which is a sign of the gradual evolution of quantum dot confinement (Palaniselvam et al. 2014; Qu et al. 2016). In addition, the Fig. 6 insert picture shows an optical image of N-GQDs aqueous solution excited under UV light. A dark green solution is observed with emitted blue under UV excitation (360 nm) which can be attributed to their conjugate structure, quantum size effect, surface state, and edge defect (Qu et al. 2013; Shen et al. 2017).

Photocatalysis of N-GQDs/TiO_2 nanocubic composites

The photocatalysis performance of N-GQDs/TiO_2 together with its different weight percentage is depicted in Fig. 7. A control experiment shows a minimal removal of BPA (< 1%) ensuring that the photodegradation is not endorsed by photolysis. Meanwhile, the dark reaction is carried out for a period of 24 h to ensure the adsorption-desorption equilibrium is achieved. In Fig. 7b, the results suggest that a considerably higher degradation of BPA is achieved by using the TiO_2 photocatalysts deposited with N-GQDs as compared with pure nanocubic-like TiO_2. The relatively low photocatalytic performance of TiO_2 is due to its limited photoresponse range and rapid recombination of electron-hole pairs. In fact, a complete photodegradation of BPA is achieved by 0.5 N-GQDs/TiO_2 in 30 min which is 1.85 times greater than that of pure TiO_2. This correlated well with the characterization analysis results where incorporation of N-GQDs with TiO_2 had enhanced the visible and NIR light absorption as it comprises approximately 90% of light intensity in the solar spectrum. The high weight percentage of N-GQDs has increased the light absorbance as shown in UV-vis analysis. However, the increase of N-GQDs weight percentage from 0.5 to 2.5 wt% has formed oxygen vacancies due to the high percentage of carbon in N-GQDs. Therefore, it suppressed the formation of

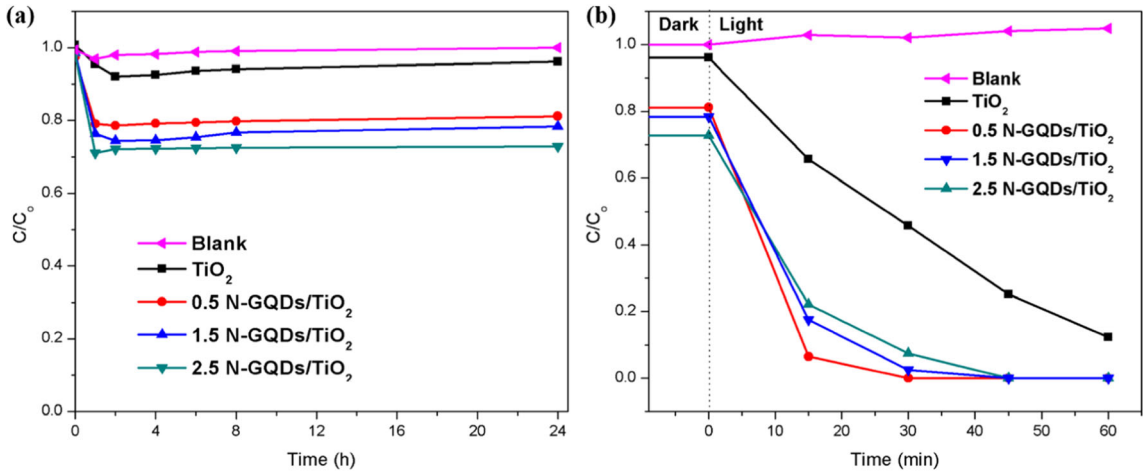

Fig. 7 **a** Dark absorption and **b** photocatalytic evaluation of TiO_2, 0.5 N-GQDs/TiO_2, 1.5 N-GQDs/TiO_2, and 2.5 N-GQDs/TiO_2

electron holes in the conduction band and leads to a reduction in active radicals' generation (Di Valentin et al. 2005; Kamisaka et al. 2005; Shen et al. 2017). As a result, 1.5 and 2.5 N-GQDs/TiO_2 requires a slightly longer duration to achieve a complete removal of BPA (45 min). This result suggests that 0.5 weight percentage is the optimum for deposition of N-GQDs onto TiO_2 for achieving an optimum photodegradation of BPA under solar irradiation.

The photodegradation rate of BPA generally fitted to a pseudo-first-order kinetic reaction $\ln(C/C_0) = kt$, where k, C, and C_0 are the apparent rate constant, initial BPA concentration, and BPA concentration after a certain time, respectively. The calculated apparent rate constants of TiO_2, 0.5 N-GQDs/TiO_2, 1.5 N-GQDs/TiO_2, and 2.5 N-GQDs/TiO_2 under solar irradiation are 0.0322 min^{-1}, 0.1824 min^{-1}, 0.1213 min^{-1}, and 0.0893 min^{-1}, respectively.

The active radical species of N-GQDs/TiO_2 nanocomposites are determined by using scavenger test. These

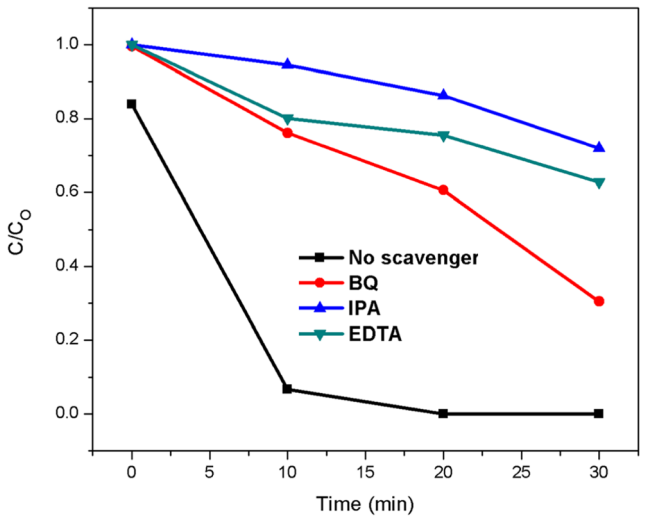

Fig. 8 Scavenger test of 0.5 N-GQDs/TiO_2 on degradation of BPA

experiments are carried out in the presence of isopropanol (IPA), EDTA disodium salt (EDTA-2Na), and benzoquinone (BQ) as scavengers to quench hydroxyl radical (·OH), photogenerated holes (h^+), and superoxide anion radical ($\cdot O_2^-$), respectively (Lei et al. 2016; Wang et al. 2016). Figure 8 indicates that all the oxidative species contribute to the BPA degradation. The contributions of these radical species $\cdot O_2^-$, h^+, and ·OH to the overall degradation of BPA about 30 min are determined to be 30%, 62%, and 77%, respectively. This result reveals that the photocatalytic degradation of BPA under sunlight irradiation in the presence of N-GQDs/TiO_2 is intimate with the photogenerated hydroxyl radical species (·OH). To distinguish the improved photocatalysis performance of N-GQDs/TiO_2, the insight understanding of materials chemistry, the formation of active radicals, and reaction between the photocatalyst and BPA pollutant are schematically presented in Fig. 9. Through the edge potential analysis, edge potentials of the conduction band (CB) and valence band (VB) of prepared N-GQDs/TiO_2 can be determined using the following equations.

$$E_{VB} = x - E^e + 0.5E_g \quad (1)$$

$$E_{CB} = E_{VB} - E_g \quad (2)$$

where E_{VB} and E_{CB} are valence band and conduction band edge potential, x is the electronegativity of the semiconductor (TiO_2 about 5.8 eV), E^e is the free electron energy on the normal hydrogen scale (about 4.5 eV vs NHE), and E_g is the band gap energy of semiconductor. Based on the equation, the calculated CB and VB edge potential against NHE of N-GQDs/TiO_2 were − 0.25 and 2.85 eV respectively. The highly positive redox potential of N-GQDs/TiO_2 encouraged the formation of highly reactive and strong oxidizing hydroxyl radicals (·OH) as redox potential of $\cdot OH/OH^-$ is 1.99 eV vs NHE. Meanwhile, the photogenerated holes are also involved in the degradation of BPA. The higher negatively characteristics of as-prepared N-GQDs permitted the photoexcited electrons to

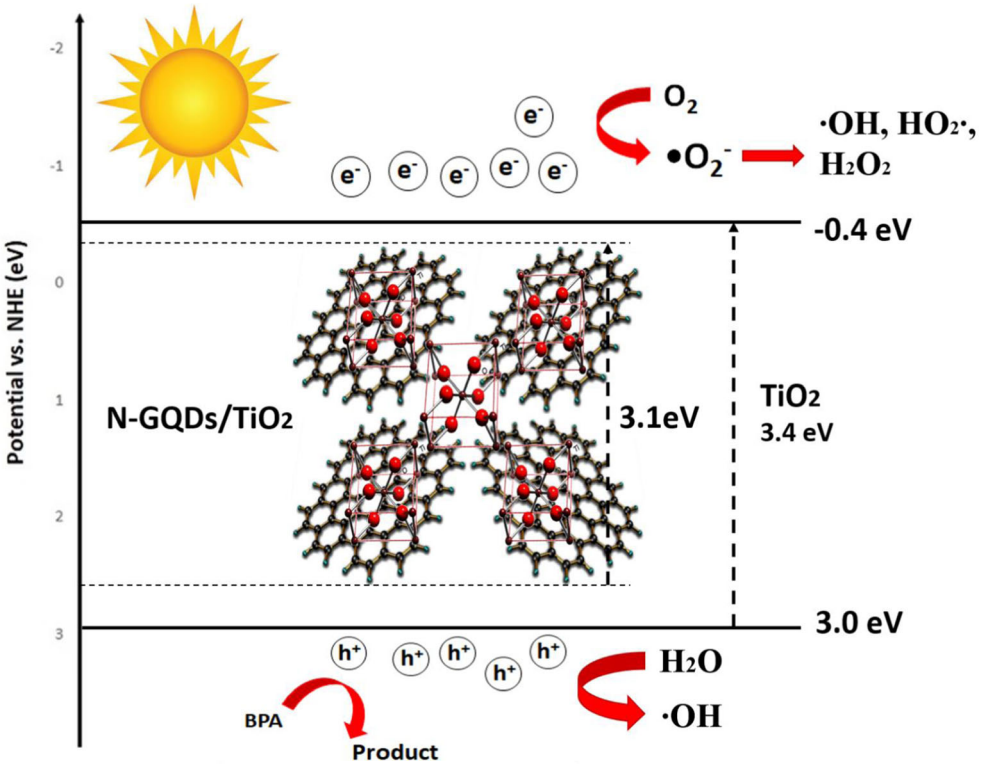

Fig. 9 Photocatalytic mechanism of 0.5 N-GQDs/TiO_2 under sunlight irradiation

be transferred from the conduction band (CB) of N-GQDs to low negative edge of CB TiO_2 (Shen et al. 2017; Zhang et al. 2017). However, the formation of active anion radical $\cdot O_2^-$ was unfavorable due to higher negativity redox potential of N-GQDs/TiO_2 against standard redox potential of $O_2/\cdot O_2^-$ (−0.33 eV) (Leong et al. 2014). The results clearly suggest that the photocatalytic process of BPA is mainly governed by hydroxyl (·OH) and holes (h^+), while superoxide ($\cdot O_2^-$) plays a weaker role as aromatic ring pollutant with low electronic density preferentially attacked by hydroxyl radicals (Palominos et al. 2008; Grabowska et al. 2017). These findings correlated well with studied characterization analysis.

Conclusion

This study demonstrates the successful synthesis of N-GQDs/TiO_2 through a simple physical mixing deposition method at room temperature. Various characterization analysis has proved the successful deposition of N-GQDs onto TiO_2 for enhanced photocatalysis performance of BPA. The synthesized 0.5 N-GQDs/TiO_2 outperforms as an optimal photocatalyst towards sunlight irradiation by achieving a complete photodegradation of BPA in a shorter duration as compared to the higher weight percentage of N-GQDs/TiO_2 and pure. This improvement is contributed to the enhanced of light absorption in the visible and NIR light region. It helps in harvesting the whole entire solar spectrum. Hence, this study provides an innovative approach which is a green, facile, and economical method to completely degrade endocrine chemical compound (BPA) by utilizing the solar energy efficiently.

Acknowledgements This research work was supported by the Universiti Tunku Abdul Rahman Research Fund, UTARRF (IPSR/RMC/UTARRF/2016-C2/L05).

References

Amorós-Pérez A, Cano-Casanova L, Lillo-Ródenas MÁ, Román-Martínez MC (2017) Cu/TiO_2 photocatalysts for the conversion of acetic acid into biogas and hydrogen. Catal Today 287:78–84

Bechambi O, Jlaiel L, Najjar W, Sayadi S (2016) Photocatalytic degradation of bisphenol A in the presence of Ce–ZnO: Evolution of kinetics, toxicity and photodegradation mechanism. Mater Chem Phys 173:95–105

Chai S, Zhao G, Zhang YN, Wang Y, Nong F, Li M, Li D (2012) Selective photoelectrocatalytic degradation of recalcitrant contaminant driven by an nP heterojunction nanoelectrode with molecular recognition ability. Environ Sci Technol 46:10182–10190

Chan DK, Cheung PL, Jimmy CY (2014) A visible-light-driven composite photocatalyst of TiO_2 nanotube arrays and graphene quantum dots. Beilstein J Nanotechnol 5:689–695

Chen Q, Zhang Y, Zhang D, Yang Y (2017) Ag and N co-doped TiO_2 nanostructured photocatalyst for printing and dyeing wastewater. J Water Process Eng 16:14–20

Chimmikuttanda SP, Naik A, Akple MS, Rajegowda RH (2017) Hydrothermal synthesis of TiO_2 hollow spheres adorned with SnO_2 quantum dots and their efficiency in the production of methanol via photocatalysis. Environ Sci Pollut Res 24:26436–26443

Chong MN, Cho YJ, Poh PE, Jin B (2015) Evaluation of titanium dioxide photocatalytic technology for the treatment of reactive Black 5 dye in synthetic and real greywater effluents. J Clean Prod 89:196–202

Chua CK, Sofer Z, Simek P, Jankovsky O, Klimova K, Bakardjieva S, Hrdličková Kučková S, Pumera M (2015) Synthesis of strongly fluorescent graphene quantum dots by cage-opening buckminsterfullerene. ACS Nano 9:2548–2555

Das R, Dhar N, Bandyopadhyay A, Jana D (2016) Size dependent magnetic and optical properties in diamond shaped graphene quantum dots: a DFT study. J Phys Chem Solids 99:34–42

Di Valentin C, Pacchioni G, Selloni A (2005) Theory of carbon doping of titanium dioxide. Chem Mater 17:6656–6665

Dominguez S, Huebra M, Han C, Campo P, Nadagouda MN, Rivero MJ, Ortiz I, Dionysiou DD (2017) Magnetically recoverable TiO_2-WO_3 photocatalyst to oxidize bisphenol A from model wastewater under simulated solar light. Environ Sci Pollut Res 24:12589–12598

Dong Y, Lin J, Chen Y, Fu F, Chi Y, Chen G (2014) Graphene quantum dots, graphene oxide, carbon quantum dots and graphite nanocrystals in coals. Nanoscale 6:7410–7415

González-Pedro V, Zarazua I, Barea EM, Fabregat-Santiago F, de la Rosa E, Mora-Seró I, Giménez S (2014) Panchromatic solar-to-H_2 conversion by a hybrid quantum dots–dye dual absorber tandem device. J Phys Chem C 118:891–895

Grabowska E, Marchelek M, Klimczuk T, Lisowski W, Zaleska-Medynska A (2017) TiO_2/$SrTiO_3$ and $SrTiO_3$ microspheres decorated with Rh, Ru or Pt nanoparticles: highly UV–vis responsible photoactivity and mechanism. J Catal 350:159–173

Guerra P, Kim M, Teslic S, Alaee M, Smyth SA (2015) Bisphenol-A removal in various wastewater treatment processes: operational conditions, mass balance, and optimization. J Environ Manag 152:192–200

Henderson MA (2011) A surface science perspective on photocatalysis. Surf Sci Rep 66:185–297

Hund-Rinke K, Simon M (2006) Ecotoxic effect of photocatalytic active nanoparticles (TiO_2) on algae and daphnids (8 pp). Environ Sci Pollut Res 13:225–232

Huy NX, Phuong DTT, Van Minh N (2017) A study on structure, morphology, optical properties, and photocatalytic ability of $SrTiO_3$/TiO_2 granular composites. Phys B Condens Matter 532:37–41

Kamisaka H, Adachi T, Yamashita K (2005) Theoretical study of the structure and optical properties of carbon-doped rutile and anatase titanium oxides. J Chem Phys 123:084704

Kaur M, Verma NK (2014) $CaCO_3$/TiO_2 nanoparticles based dye sensitized solar cell. J Mater Sci Technol 30:328–334

Lei ZD, Wang JJ, Wang L, Yang XY, Xu G, Tang L (2016) Efficient photocatalytic degradation of ibuprofen in aqueous solution using novel visible-light responsive graphene quantum dot/$AgVO_3$ nanoribbons. J Hazard Mater 312:298–306

Leong KH, Monash P, Ibrahim S, Saravanan P (2014) Solar photocatalytic activity of anatase TiO_2 nanocrystals synthesized by non-hydrolitic sol–gel method. Sol Energy 101:321–332

Li J, Wang Y, Tian Y, He X, Yang P, Yuan M, Cao Y, Lyu J (2018) Crystallization of microporous TiO_2 through photochemical deposition of Pt for photocatalytic degradation of volatile organic compounds. Environ Sci Pollut Res 25:15662–15679

Liu G, Ma J, Li X, Qin Q (2009) Adsorption of bisphenol A from aqueous solution onto activated carbons with different modification treatments. J Hazard Mater 164:1275–1280

Mahmood T, Cao C, Tahir M, Idrees F, Ahmed M, Tanveer M, Aslam I, Usman Z, Ali Z, Hussain S (2013) Electronic, elastic, acoustic and optical properties of cubic TiO_2: A DFT approach. Physica B 420: 74–80

Martins NC, Ângelo J, Girão AV, Trindade T, Andrade L, Mendes A (2016) N-doped carbon quantum dots/TiO_2 composite with improved photocatalytic activity. Appl Catal B Environ 193:67–74

Miloua R, Kebbab Z, Benramdane N, Khadraoui M, Chiker F (2011) Ab initio prediction of elastic and thermal properties of cubic TiO_2. Comput Mater Sci 50:2142–2147

Min S, Hou J, Lei Y, Ma X, Lu G (2017) Facile one-step hydrothermal synthesis toward strongly coupled TiO_2/graphene quantum dots photocatalysts for efficient hydrogen evolution. Appl Surf Sci 396: 1375–1382

Palaniselvam T, Valappil MO, Illathvalappil R, Kurungot S (2014) Nanoporous graphene by quantum dots removal from graphene and its conversion to a potential oxygen reduction electrocatalyst via nitrogen doping. Energy Environ Sci 7:1059–1067

Palominos R, Freer J, Mondaca MA, Mansilla HD (2008) Evidence for hole participation during the photocatalytic oxidation of the antibiotic flumequine. J Photochem Photobiol A-Chem 193:139–145

Pan D, Zhang J, Li Z, Wu M (2010) Hydrothermal route for cutting graphene sheets into blue luminescent graphene quantum dots. Adv Mater 22:734–738

Pan D, Jiao J, Li Z, Guo Y, Feng C, Liu Y, Wang L, Wu M (2015) Efficient separation of electron–hole pairs in graphene quantum dots by TiO_2 heterojunctions for dye degradation. ACS Sustain Chem Eng 3:2405–2413

Park H, Park Y, Kim W, Choi W (2013) Surface modification of TiO_2 photocatalyst for environmental applications. J Photochem Photobiol C 15:1–20

Pelaez M, Nolan NT, Pillai SC, Seery MK, Falaras P, Kontos AG, Dunlop PS, Hamilton JW, Byrne JA, O'shea K, Entezari MH (2012) A review on the visible light active titanium dioxide photocatalysts for environmental applications. Appl Catal B Environ 125:331–349

Qu D, Zheng M, Du P, Zhou Y, Zhang L, Li D, Tan H, Zhao Z, Xie Z, Sun Z (2013) Highly luminescent S, N co-doped graphene quantum dots with broad visible absorption bands for visible light photocatalysts. Nanoscale 5:12272–12277

Qu A, Xie H, Xu X, Zhang Y, Wen S, Cui Y (2016) High quantum yield graphene quantum dots decorated TiO_2 nanotubes for enhancing photocatalytic activity. Appl Surf Sci 375:230–241

Rajabi HR, Farsi M (2015) Effect of transition metal ion doping on the photocatalytic activity of ZnS quantum dots: synthesis, characterization, and application for dye decolorization. J Mol Catal A Chem 399:53–61

Rajabi HR, Farsi M (2016) Study of capping agent effect on the structural, optical and photocatalytic properties of zinc sulfide quantum dots. Mater Sci Semicond Process 48:14–22

Rajabi HR, Khani O, Shamsipur M, Vatanpour V (2013) High-performance pure and Fe3+-ion doped ZnS quantum dots as green nanophotocatalysts for the removal of malachite green under UV-light irradiation. J Hazard Mater 250:370–378

Ribao P, Rivero MJ, Ortiz I (2017) TiO_2 structures doped with noble metals and/or graphene oxide to improve the photocatalytic degradation of dichloroacetic acid. Environ Sci Pollut Res 24:12628–12637

Rodenas P, Song T, Sudhagar P, Marzari G, Han H, Badia-Bou L, Gimenez S, Fabregat Santiago F, Mora Sero I, Bisquert J, Paik U (2013) Quantum dot based heterostructures for unassisted photoelectrochemical hydrogen generation. Adv Energy Mater 3: 176–182

Roushani M, Mavaei M, Rajabi HR (2015) Graphene quantum dots as novel and green nano-materials for the visible-light-driven photocatalytic degradation of cationic dye. J Mol Catal A Chem 409:102–109

Roy N, Sohn Y, Pradhan D (2013) Synergy of low-energy {101} and high-energy {001} TiO_2 crystal facets for enhanced photocatalysis. ACS Nano 7:2532–2540

Safardoust-Hojaghan H, Salavati-Niasari M (2017) Degradation of methylene blue as a pollutant with N-doped graphene quantum dot/titanium dioxide nanocomposite. J Clean Prod 148:31–36

Shen K, Xue X, Wang X, Hu X, Tian H, Zheng W (2017) One-step synthesis of band-tunable N, S co-doped commercial TiO_2/graphene quantum dots composites with enhanced photocatalytic activity. RSC Adv 7:23319–23,327

Taheri ME, Petala A, Frontistis Z, Mantzavinos D, Kondarides DI (2017) Fast photocatalytic degradation of bisphenol A by Ag_3PO_4/TiO_2 composites under solar radiation. Catal Today 280:99–107

Tian H, Shen K, Hu X, Qiao L, Zheng W (2017) N, S co-doped graphene quantum dots-graphene-TiO_2 nanotubes composite with enhanced photocatalytic activity. J Alloys Compd 691:369–377

Wang G, Wang H, Ling Y, Tang Y, Yang X, Fitzmorris RC, Wang C, Zhang JZ, Li Y (2011) Hydrogen-treated TiO_2 nanowire arrays for photoelectrochemical water splitting. Nano Lett 11:3026–3033

Wang J, Li C, Cong J, Liu Z, Zhang H, Liang M, Gao J, Wang S, Yao J (2016) Facile synthesis of nanorod-type graphitic carbon nitride/Fe_2O_3 composite with enhanced photocatalytic performance. J Solid State Chem 238:246–251

Wu W, Shan G, Wang S, Zhu L, Yue L, Xiang Q, Zhang Y, Li Z (2016) Environmentally relevant impacts of nano-TiO_2 on abiotic degradation of bisphenol A under sunlight irradiation. Environ Pollut 216:166–172

Xie H, Hou C, Wang H, Zhang Q, Li Y (2017) S, N Co-doped graphene quantum dot/TiO_2 composites for efficient photocatalytic hydrogen generation. Nanoscale Res Lett 12:400

Xu Q, Yu J, Zhang J, Zhang J, Liu G (2015) Cubic anatase TiO_2 nanocrystals with enhanced photocatalytic CO_2 reduction activity. Chem Commun 51:7950–7953

Yamanaka H, Moriyoshi K, Ohmoto T, Ohe T, Sakai K (2008) Efficient microbial degradation of bisphenol A in the presence of activated carbon. J Biosci Bioeng 105:157–160

Yu S, Zhong YQ, Yu BQ, Cai SY, Wu LZ, Zhou Y (2016) Graphene quantum dots to enhance the photocatalytic hydrogen evolution efficiency of anatase TiO_2 with exposed {001} facet. Phys Chem Chem Phys 18:20338–20344

Zhang Y, Qi F, Li Y, Zhou X, Sun H, Zhang W, Liu D, Song XM (2017) Graphene oxide quantum dot-sensitized porous titanium dioxide microsphere: Visible-light-driven photocatalyst based on energy band engineering. J Colloid Interface Sci 498:105–111

Zhao L, Xiao X, Peng L, Gu FL, Zhang RQ (2014) Visible-light photocatalytic mechanism of bisphenol-A on nano-Bi_2O_3: a combined DFT calculation and experimental study. RSC Adv 4:10343–10349

Zhu H, Liu A, Xu Y, Shan F, Li A, Wang J, Yang W, Barrow C, Liu J (2015) Graphene quantum dots directly generated from graphite via magnetron sputtering and the application in thin-film transistors. Carbon 88:225–232